Spring 2017

Multiplexed Sensor Array for Accurate Time-of-Wetness (TOW) Measurement

Nathaniel G. Sutton
University of Akron, Dept. of Chemical and Biomolecular Engineering, ngs10@zips.uakron.edu

Hongbo Cong
The University of Akron, hcong@uakron.edu

Jiang John Zhe
The University of Akron, jzhe@uakron.edu

Shengxi Li
The University of Akron, sli17@uakron.edu

Xiaoliang Zhu
The University of Akron, xz31@zips.uakron.edu

Multiplexed Sensor Array for Accurate Time-of-Wetness (TOW) Measurement

Honors Research Project in Corrosion Engineering - 4250:497

Recipient: Department of Chemical and Biomolecular Enginering

Primary Author: Nathaniel Sutton

Contributing Authors: Xiaoliang Zhu, Shengxi Li, Jiang Zhe, and Hongbo Cong

Date: 12 April 2017

Abstract

In this work, we use electrochemical impedance spectroscopy (EIS) to observe the response of a single, photo-lithographically created, interdigital transducer (IDT) sensor, dimensions 6mm X 6 mm, with capacitive elements 70μm X 500 nm. The IDT was exposed to different wetting conditions, droplets of DI water, 0.1 M NaCl, and 0.6 M NaCl, in volumes of 0.1, 0.3, 1, and 5 μL. Deliquescence of solid NaCl salt particles in a dynamic-humidity (%RH Increasing, 33% to 85%) atmosphere is examined. Equivalent circuit fitting of impedance spectra suggests linear trends for the capacitive equivalent circuit element parameters and a decaying logarithmic trend for the resistive element, with respect to electrolyte concentration vs. area of wetting. The sensor development process includes a 1 by 5 proof-of-concept linear array, and the eventual goal of a 5 by 5 matrix array. The array sensor aims to (1) determine the overall fraction of wet surface area, and (2) distinguish between electrolytes of varying conductivity, in a 2-dimensional gradient across a surface.

Executive Summary

Problem Statement

Time-of-wetness (TOW) is a critical factor affecting atmospheric corrosion. Current TOW sensor capabilities are limited, measuring galvanic current, electrical resistance, or impedance, and determining TOW by comparing the sensor output to arbitrary threshold values. Coated, resistance-based TOW sensors require time for water uptake, and may not detect rapid wetting events. Galvanic TOW sensors are consumed by use and requiring replacement; they are subject to errors from hygroscopic corrosion products. Our hypothesis was that EIS evaluation of a sensor could delineate between conditions of differing electrolyte concentration and droplet size.

Summary of Results

EIS was conducted on a single-IDT sensor, approx. 6X6 mm, with elements 70µm X 500 nm, subject to 0.1, 0.3, 1.0, and 5.0 µL droplets of DI water, 0.1 M and 0.6M NaCl. Comparison of spectra revealed differences between the droplet volumes and concentrations studied. Circuit fitting showed linear trends in $C_{DROPLET}$ and Q_{DL} (vs droplet area) with slopes increasing with concentration, and a decreasing logarithmic trend for $R_{DROPLET}$. These variables are defined in *Experimental Methods*. Q_{DL} ranged from 19.3 $nF \cdot s^{(n-1)}$ (smallest DI water droplet) to 511.8 $nF \cdot s^{(n-1)}$ (largest 0.6 M NaCl droplet), with an average n of 0.594, from a range of 0.53-0.67. $C_{DROPLET}$ ranged from 0.823 pF to 33.93 pF, although trends in this parameter are not as distinguishable for the smallest droplets. $R_{DROPLET}$ varied from 138 kΩ (smallest DI water droplet) to 2.0 kΩ (largest NaCl droplets). Deliquescence of dry NaCl crystals in dynamic humidity conditions was observed in the range of 71-75%RH, which differs slightly from the literature value of 75.3%RH, yet demonstrates sensor viability in dynamic conditions.

Conclusions

Interrogation of the sensor via EIS allows simultaneous determination of wetted area and conductivity of electrolyte. Collected spectra fit to the predicted impedance of proposed equivalent circuits rather well. An alternative equivalent circuit, accounting for the effects of metal-solution interface (Q_{DL} & R_P) in series with the bulk effects ($C_{DROPLET}$ & $R_{DROPLET}$), is also suggested, and will be the subject of ongoing investigation. Observation of these trends suggests that it is possible to differentiate between different sizes of droplets and concentrations of electrolytes on the single-IDT sensor, by using EIS to characterize wetting events.

Implications

The multiplexed IDT array described herein aims to rectify shortcomings of current sensors, and generate reliable field data, providing information on atmospheric corrosion. Two designs for a novel sensor array are proposed, with multiple IDT sensors arranged in both 1-D (1X5) and 2-D (5X5). These array designs seek to successfully characterize non-uniform wetting conditions across a surface.

This honors project has enhanced my ability to conduct small scale (μL & μm-sized) experiments with precision. It has solidified my technical understanding of EIS and allowed me to develop equivalent circuit models for real systems with confidence, pulling a basis from literature sources in similar applications. As a result of presenting this work at NACE Corrosion 2017 and subjecting the technical paper to NACE symposium review, I have gained valuable experience in academic presentations and written technical correspondence. The results of this project offer the benefit of accurate atmospheric corrosion characterization. The cost of corrosion has been quantified by NACE in their recent *IMPACT* study as US$2.5 trillion globally, not to

include the costs associated with asset failure as a result of corrosion[17]. A large portion is spent on corrosion prevention efforts, including protective coatings, galvanization, corrosion inhibition, etc. In some cases, little information about the severity of atmospheric corrosion is known at construction; as a result, owners have little technical guidance available for selecting corrosion prevention tools. This project aims to partially fill that void, thereby allowing more data-driven decisions to be made.

Recommendations

Additional research should be conducted on the recently-constructed 3-IDT sensor panel. Although this prototype does not integrate the 3 sensors adjacent to each other, it grants the ability to verify initial results on different IDT sensors simultaneously. As a result, it allows the development of signal processing which will be necessary for the development of the eventual 5X5 array. Further investigation should evaluate more and less concentrated electrolytes, and additional droplet sizes. A variety of electrolyte species (i.e. other than NaCl) should also be examined to test the relationships proposed. The equivalent circuit proposed in the discussion section of this report should be scrutinized for its applicability to the collected data.

Students working on technology development projects in the future are advised to learn how their technology is created. In the case of the sensor examined in this work, I was not allowed to operate the photo-lithography equipment used to create the device. It was therefore challenging to gain a full understanding of the limitations of the pre-existing design. Future students should try to observe the creation of their prototype, or even possibly make the device themselves.

Introduction

A multitude of interrelated factors influence atmospheric corrosion of metals, including time-of-wetness (TOW), relative humidity (%RH), structure geometry, and the presence contaminant particles, among others[1,2,3,4]. These variables are often very complex; for instance, different areas of the same structure may experience different wetting patterns, surface temperatures, and local relative humidity, altering material behavior[5,6,7,3]. Furthermore, the size, dispersion, and hygroscopic nature of contaminant particles on the surface can influence wetting behavior, complicating atmospheric corrosion characterization[8,2,6]. Researchers have also identified the influence of TOW and %RH parameters on other damage mechanisms, including crevice-corrosion and pitting corrosion[9]. Accurate determination of TOW and other variables can provide better information on the corrosion mechanism, guiding decisions on laboratory testing (e.g. coating evaluation), asset protection, life determination, and computational modelling.

Scope

The present work characterizes the electrochemical behavior of a single TOW sensor with respect to varying electrolyte concentrations and volumes, and discusses feasibility of constructing a multiplexed sensor array for better measurement. Alternating current electrical impedance, or electrochemical impedance spectroscopy (EIS), has been described in the literature [3,10], and is the signal-response method of choice for the IDT in this investigation.

Background

Existing TOW sensors are currently limited in accuracy of wetness detection. The most prevalent sensors measure (1) galvanic current, (2) resistance, or (3) electrical impedance between interwoven electrodes to determine whether or not a material is "wet," [5,7]. Wetness is determined

by comparing the sensor output to a predefined threshold value. In many cases, such parameters correlate poorly to physical corrosion phenomena [2,3]. Analysis methods which attempt to correlate sensor output to TOW on the surface often introduce additional error; in fact, research has shown the limitations of multiple standard methods of TOW determination [2,4]. Coated, resistance-based TOW sensors time for water uptake; if a rapid wet/dry cycle occurs, delayed water uptake through the coating can prevent the moisture from being detected, Figure 1.
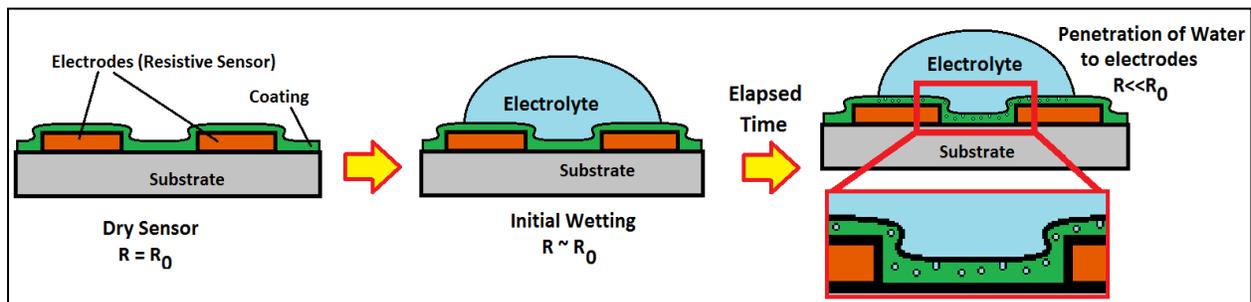
Figure 1: Mechanism of wetness detection for coated, DC resistance-based TOW sensor.

Some common TOW sensors that are galvanic in nature are consumed by use over time, requiring replacement. Hygroscopic corrosion products from the galvanic action of these sensors can become deposited between the electrodes, holding moisture in the gap, while the remainder of the surface of the structure may be dry, Figure 2 [5,7].
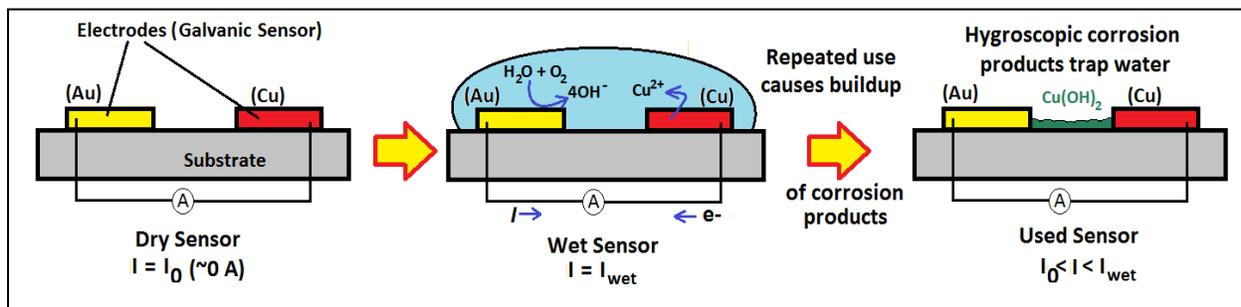
Figure 2: Mechanism of wetness detection for galvanic current TOW sensor, showing the process by which hygroscopic corrosion products may accumulate.

Finally, the resolution of the sensors (i.e. the minimum droplet or salt particle size that can be detected) is limited by the spacing of the electrode [2,10]. The multiplexed impedance-based sensor array, which we are developing, aims to rectify these issues.

Experimental Methods

Sensor Design & Construction

The TOW sensor used in this investigation is made of solid chromium metal, printed photo-lithographically on a polyimide substrate, according to the schematic shown in Figure 3 [11]. To begin, a thin film of chromium metal, between 500 nm and 1 μm thick, is deposited on the substrate. In step 1, a chemically-resistant, Ultraviolet (UV) sensitive coating is applied to cover the chromium metal. In step 2, a mask is applied, which blocks UV radiation from reaching the sensitive coating. The mask is designed to have the same pattern as the final IDT sensor. UV radiation, as shown in the schematic, alters the sensitive coating such that it can be washed away by chemical development in step 3. The remaining coating is essentially a negative of the IDT sensor pattern. When the surface is treated with an etchant, as in step 4, the exposed chromium is dissolved, while chromium under the intact chemically-resistant coating remains adhered to the substrate. In step 5, the surface is again irradiated with UV and chemically developed [11]. The result is an IDT pattern with behavior similar to that of an ideal capacitor. The approximate dimensions of electrodes used in this investigation (Figure 4) are 6mm long X 70 μm wide X 0.5-1.0 μm thick, with an inter-electrode gap of 80 μm.
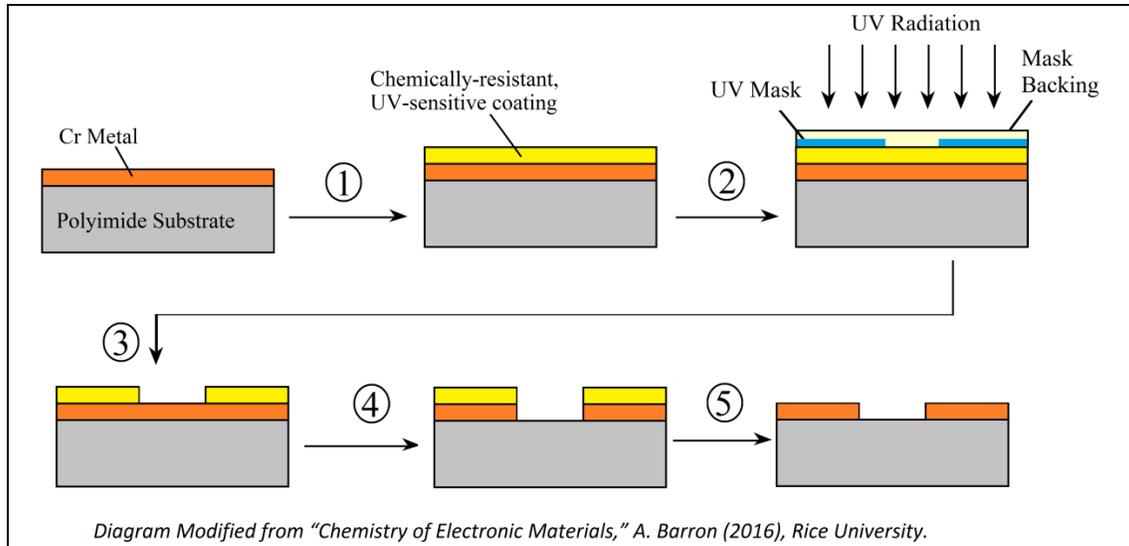
Figure 3: Photolithography manufacturing process used for creating TOW IDT sensor[11].

Figure 4: Macroscopic view of TOW single-IDT sensor.

Environmental Control Chamber

The sensor was placed in a sealable humidity chamber with 1.7 L volume. At the bottom of this container was a beaker containing saturated $MgCl_2$ solution for humidity control [9,12]. A tube, outfitted with hose clamp, was used to add deionized (DI) water to the beaker solution. Dilution of the concentrated $MgCl_2$ solution (at equilibrium saturation of 33%RH) results in an increase in %RH. Throughout experiments, DI water was added to increase %RH; additional saturated $MgCl_2$ was used to decrease %RH. A magnetic stirring plate was used to agitate the solution and maintain the desired humidity level. Figure 5 shows this general experimental setup.
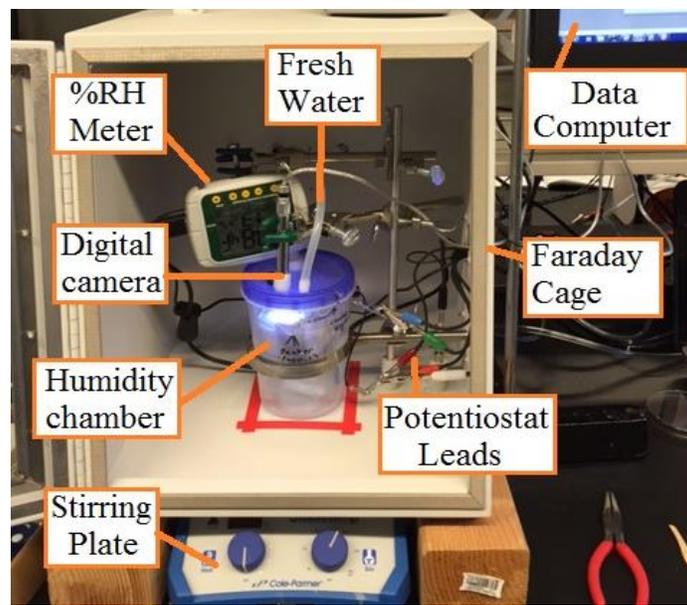
Figure 5: Benchtop setup used for all experiments, showing key components of setup.

Before each experiment, the sensor was scrubbed with a regimen of (1) DI water, (2) acetone, (3) ethanol, (4) DI water, before drying in 99.999% Argon. This cleaning sequence was performed to give a baseline surface condition (free of particles, dirt, previous experiment electrolyte residue, etc.) in each test. After cleaning, the sensor was mounted in the humidity chamber.

To determine the effects of droplet size and electrolyte concentration, 4 different droplet volumes (0.1, 0.3, 1.0, 5.0 μL) and 3 electrolytes (DI Water, 0.1M NaCl, 0.6M NaCl) were examined. Volumes were measured via micro-syringe and deposited onto the center of the IDT-sensor's area after RH had stabilized. Droplets were in an atmosphere with relative humidity in equilibrium with the concentration (e.g. the 0.1M NaCl droplet was above a continuously-agitated solution of 0.1M NaCl). The position of droplets on the sensor is shown in Figure 6.
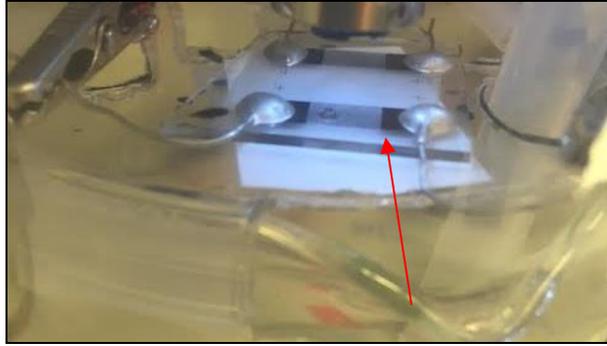
Figure 6: Close-up view of sensor, during experiment, showing small electrolyte droplet (red arrow) on the single-IDT TOW. Beaker below sensor holds the humidity control solution.

Deliquescence of NaCl crystals was also monitored using the single sensor. Salt particles were formed by placing a 1.0 μL droplet of 1.0 M NaCl (*in water*) on the sensor and allowing it to dry in air. The humidity in the chamber was rapidly increased in each case, by first placing 10 mL of saturated $MgCl_2$ in the beaker, then quickly adding approximately 150 mL of DI water to the control solution. To ensure the most accurate measurement of %RH in the immediate proximity of the sensor, the %RH meter was positioned to within 1 inch of the sensor being tested.

Equivalent Circuits Utilized for Analysis
All tests used electrochemical impedance spectroscopy (EIS) to analyze the wetting conditions on the sensor. EIS was measured over various frequency ranges (including 100 kHz - 1 Hz, 100 kHz - 1000 Hz, or 1 MHz - 100 Hz,) depending on nature of the test and the rapidity of changes in wetness condition(s). Frequency ranges similar to this have been previously tested [3,10]. To explain the impedance (Z) response observed in each test, the equivalent circuits shown in Figure 7 were used. The air (i.e. dry sensor) and substrate were treated as capacitors, with impedance response (Z_C) governed by Equation 1, where j is the imaginary vector, ω is the frequency in radians per second, and C is the capacitance, in Farads.

$$Z_C = (j\omega C)^{-1} \tag{1}$$

In the case of a wetted sensor, the imperfect dielectric behavior of the metal-solution interfaces precludes the use of pure capacitor, and the impedance of the electric double layer is better modeled by a constant phase element (CPE). The impedance of a CPE (Z_{CPE}) is calculated by Equation 2, where Q (effective capacitance) is the CPE parameter similar to capacitance and n is a positive parameter less than 1. When wet, current also flows through the electrolyte, a resistor.

$$Z_{CPE} = (j\omega)^{-n}(Q)^{-1} \tag{2}$$

The impedance of a resistor (Z_R) is simply equal to its DC resistance, as shown in Equation 3.

$$Z_R = R \tag{3}$$

In normal 3-electrode EIS, the circuit exists between the reference (RE) and the working (WE) electrode. The counter electrode (CE) only exists to sinusoidally manipulate the voltage of the WE, so that the current response can be measured in order to determine the impedance vector at each frequency. In such a setup, the CE's potential is varied as necessary in order to drive the voltage of the WE; no current actually flows between the WE and RE. The TOW sensor's scenario of 2-electrode EIS is different insomuch as the circuit exists between a combined counter/reference (C/RE) and the WE. Thus, current (AC) flows between the C/RE and the WE, through the solution ($R_{DROPLET}$). The entire phase delay is not fully accounted for with only the Q_{DL} capacitor; the addition of an ideal capacitor (e.g. $C_{DROPLET}$) to the circuit allows phase delay from the AC electric field across the bulk solution (i.e. not just within the double layers) to be quantified, as suggested by other researchers [15]. Thus, the capacitive properties of the circuit

incorporate both the Q_{DL} and $C_{DROPLET}$. The phase delay caused by $C_{DROPLET}$ may be attributed to the alignment of water molecule polarity with the AC electric field [16].
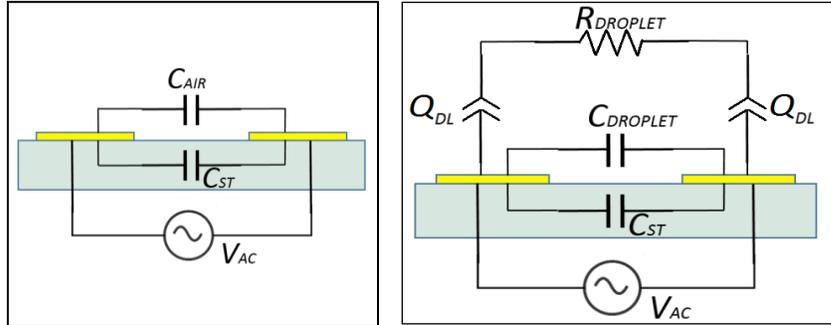
Figure 7: Equivalent Circuits used to analyze dry sensor (left) and wet sensor (right) responses. C (e.g. $C_{DROPLET}$, C_{ST}, C_{AIR}) denotes a capacitive circuit element modelled by ideal dielectric, Eq. (1). Q (e.g. Q_{DL}) denotes an effective capacitance modelled by constant phase element, Eq. (2)

Data and Results

Effect of Droplet Size & Electrolyte Concentration

Characteristic appearance of the four droplet volumes (0.1, 0.3, 1.0, 5.0 µL) are shown in Figure 8. The sensor can be thought of as 2 combs with interlocking fingers. As visual analysis indicates, an increasing droplet size corresponds to a greater number of capacitor fingers in contact with the electrolyte, and a larger surface area of the capacitor engaged through which the AC field may pass. Figure 9 shows Bode impedance & phase plots for DI water droplets of different volume on the sensor. Figure 10 shows the same plots for 0.6 M NaCl droplets of different volumes, at their own equilibrium relative humidity. Figures visualize trends to demonstrate the sensitivity of the sensor & EIS analysis method to changes in droplet size and concentration. The trends on each figure are relevant in the discussion of the equivalent circuit

model output. Impedance curves calculated from fitting parameters are also plotted to demonstrate viability of equivalent circuit fitting analysis.
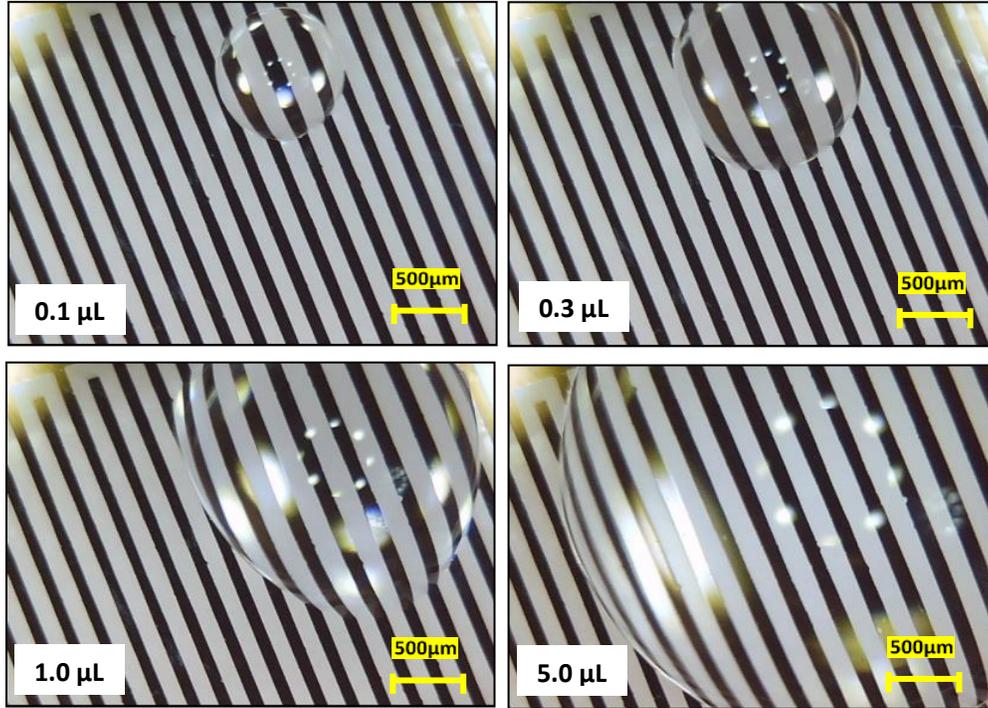
Figure 8: Approximate size and appearance of the 4 droplet volumes used in experiments.
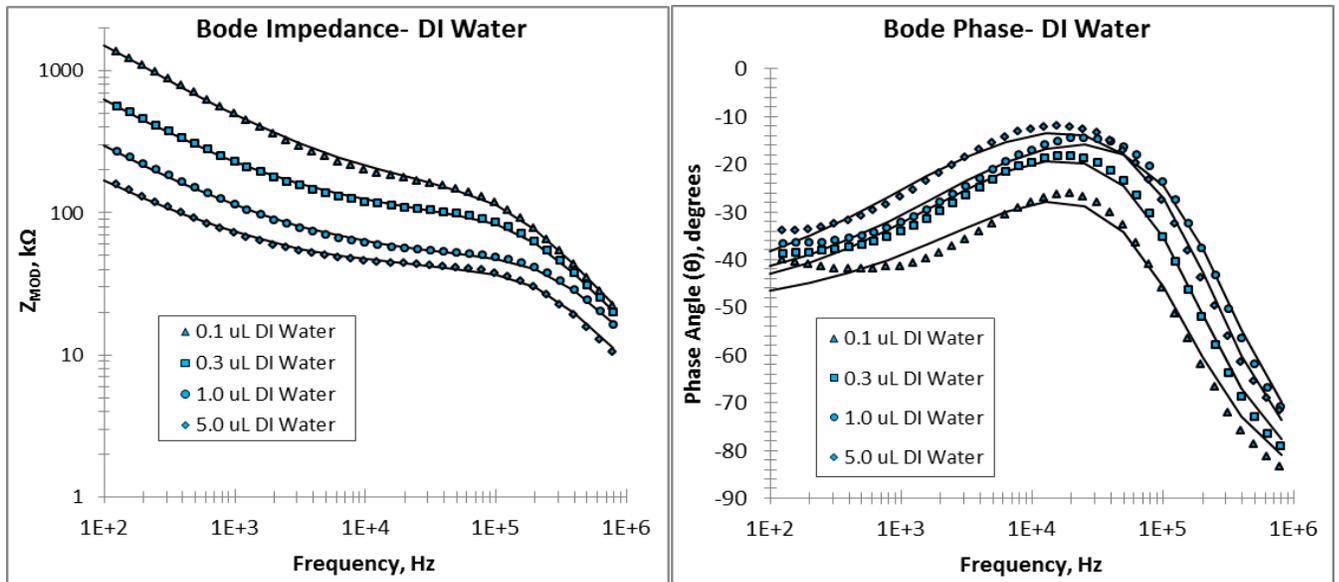
Figure 9: Bode impedance (left) & phase (right) for DI water droplets of varying volume.
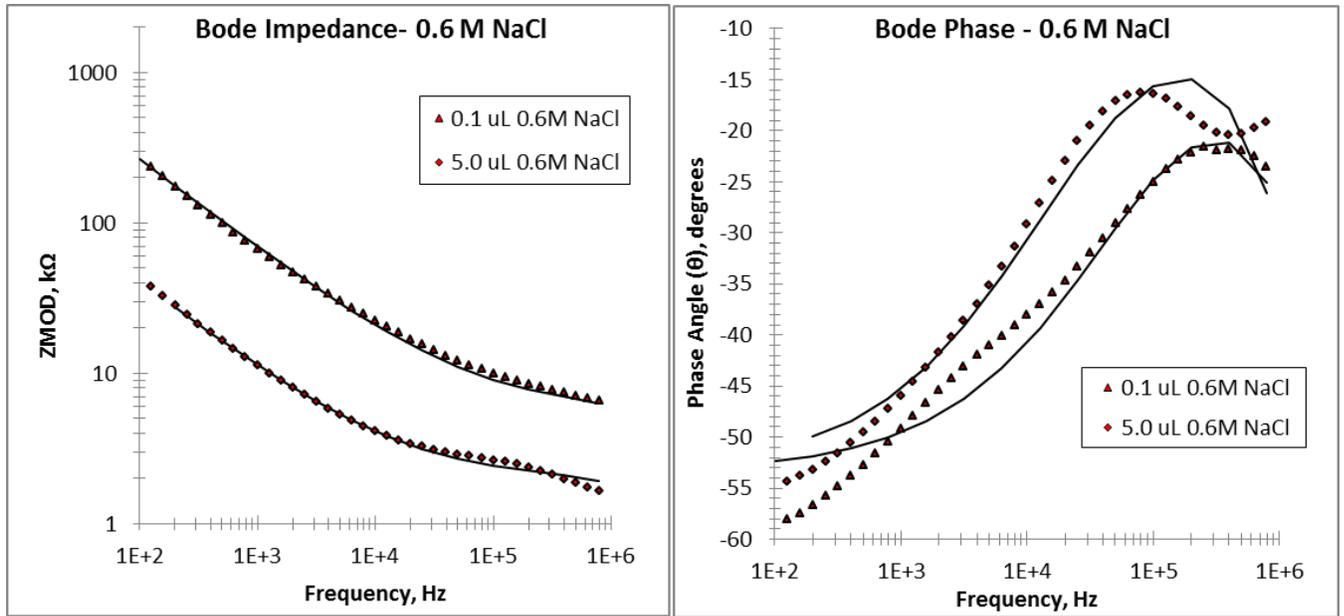
Figure 10: Bode impedance (left) & phase (right) for 0.6 M NaCl droplets of varying volume.

Figures 9 & 10 show that, at all frequencies in the spectrum, in both DI water and 0.6 M NaCl electrolytes, the total impedance magnitude, Z_{MOD} decreases as the droplet volume (and thus wetted area) increases. At frequencies near 1 MHz, the impedance response of the sensor in DI water, Figure 9, is similar to that of a pure capacitor (near -90° phase angle). The impedance of the sensor in 0.6 M NaCl, Figure 10, is more of a resistor (approximately -10° to -20° phase angle). In the case of DI water, the divergence between Z_{MOD} values is greatest at lower frequencies; this is not observed for saltwater.

Figure 11 shows Bode impedance & phase plots for small droplets (0.1 μL) of various concentrations. Figure 12 shows the same plots for large droplets (5.0 μL) of the same three concentrations.
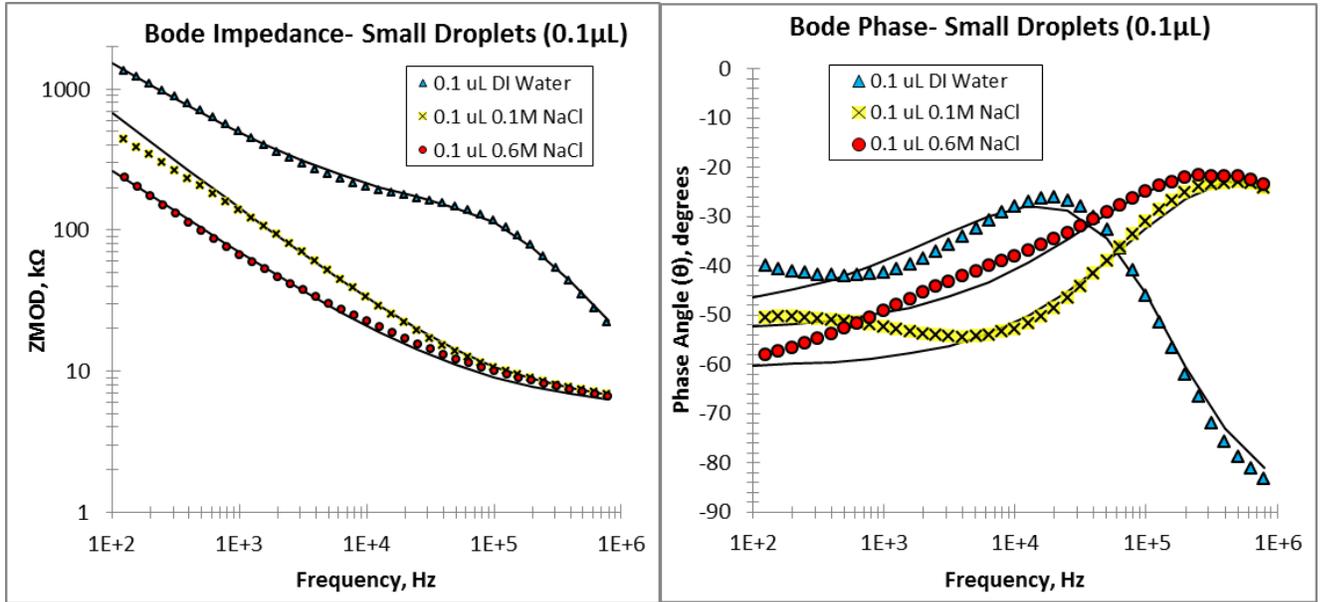
Figure 11: Bode impedance (left) & phase (right), small droplets (0.1 μL).
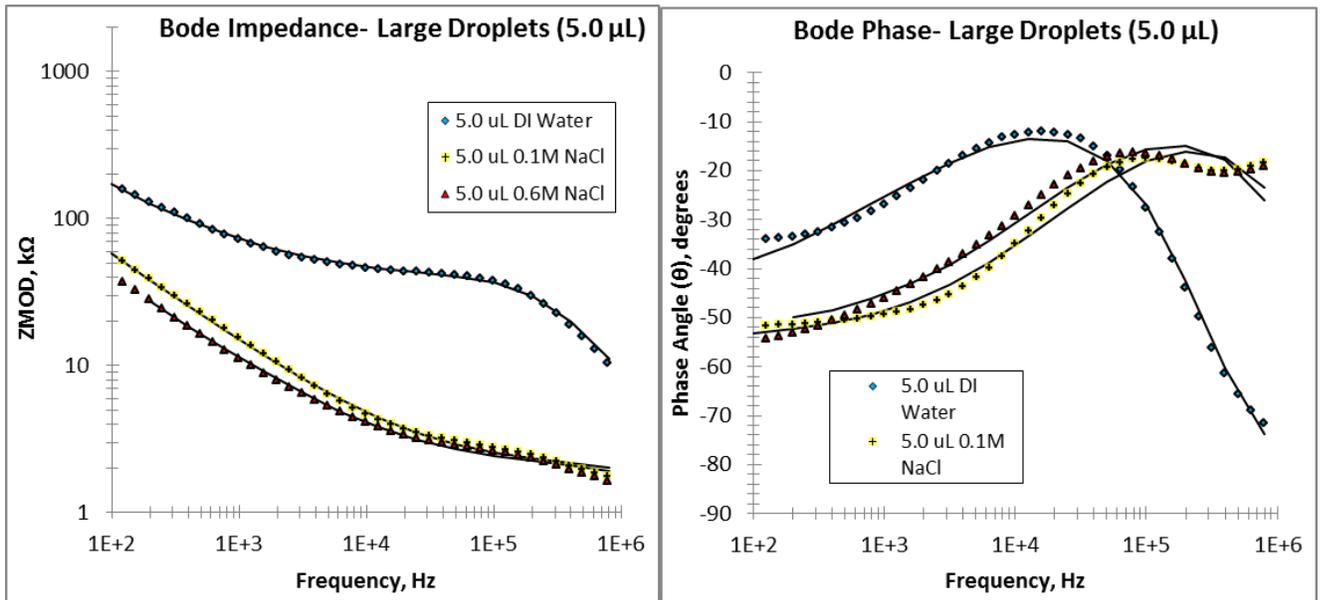
Figure 12: Bode impedance (left) & phase (right), large droplets (5.0 μL).

In Figures 11 & 12, the value of Z_{MOD} is similar for both dilute (0.1 M NaCl) and concentrated (0.6 M NaCl) saltwater at high frequencies, while the value of Z_{MOD} for DI water droplet of the same size is much closer to the response of the dry sensor in air. The Z_{MOD} values for dilute &

concentrated saltwater do not diverge significantly for either small or large droplets until the frequency is less than about 1 kHz. However, the phase angle plots for dilute & concentrated saltwater vary at frequencies below 100 kHz. Furthermore, the shapes of the Bode phase angle plots for both dilute & concentrated saltwater differ between large and small droplets, especially in the range of 100 kHz to 1 MHz. A commercial EIS-fitting software was used to obtain values for each of the circuit parameters identified in Figure 7. A fitting was performed on the raw data shown in Figures 9-12. The results of fitting analysis are presented in Table 1.

Table 1: Equivalent Circuit Fit Results for Droplet concentrations and Volumes Tested

Double-layer eff. capacitance (Q_{DL}), droplet resistance ($R_{DROPLET}$) & capacitance ($C_{DROPLET}$)

Electrolyte	Droplet Size	Contact Area	Q_{DL}	n	$R_{DROPLET}$	$C_{DROPLET}$
Units	*μL*	*mm^2*	*nF·s$^{(n-1)}$*	*No units*	*KΩ*	*pF*
DI Water	0.1	0.4135	19.26	0.55639	138.01	2.807
DI Water	0.3	0.8601	52.25	0.54721	92.3	3.775
DI Water	1.0	1.9192	90.33	0.56937	48.72	5.419
DI Water	5.0	5.6117	230.49	0.53046	38.596	11.739
0.1 M NaCl	0.1	0.4135	19.60	0.67345	6.422	0.823
0.1 M NaCl	0.3	0.8601	47.33	0.64554	4.305	3.606
0.1 M NaCl	1.0	1.9192	106.61	0.62365	2.904	6.827
0.1 M NaCl	5.0	5.6117	352.07	0.60856	2.033	25.46
0.6 M NaCl	0.1	0.4135	84.34	0.59261	5.982	3.378
0.6 M NaCl	0.3	0.8601	131.62	0.58844	4.703	7.277
0.6 M NaCl	1.0	1.9192	179.60	0.59458	2.855	9.402
0.6 M NaCl	5.0	5.6117	511.80	0.60141	2.052	33.93

To better observe the trends between area of wetness and concentration, the results for droplet resistance ($R_{DROPLET}$), droplet capacitance ($C_{DROPLET}$), and double-layer effective capacitance (Q_{DL}) are plotted. Limited fitting results for $C_{DROPLET}$ & Q_{DL} suggest that these parameters may follow a linear trend within the same concentration of electrolyte, with the slope vs. contacted

area (dC/dA or dQ/dA) becoming steeper for more concentrated electrolytes, Figures 13 & 14.
Contacted area was calculated by assuming hemispherical droplets. Fitting results for $R_{DROPLET}$
appear to decay to a negative natural logarithmic trend, Figure 15.
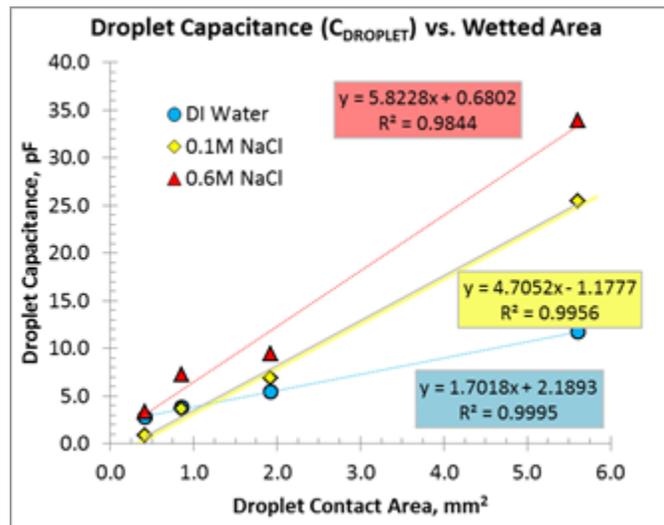
Figure 13: Plot of droplet capacitance ($C_{DROPLET}$) vs. volume; a linear relationship is postulated, where the slope increases with increasing concentration.
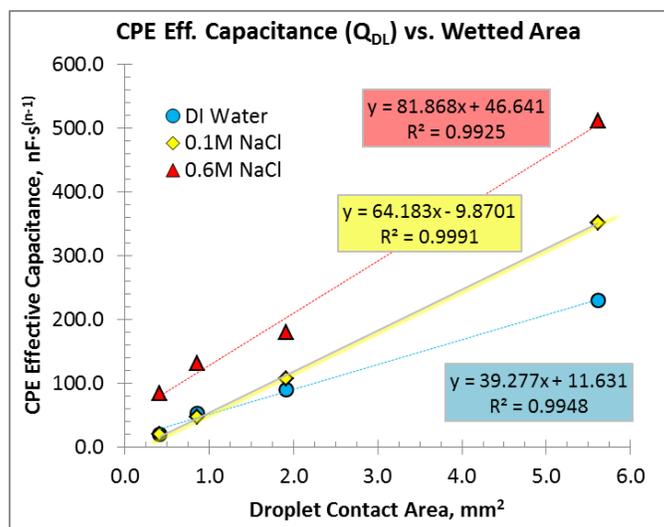
Figure 14: Plot of double-layer constant phase element parameter (Q_{DL}) vs. volume; a linear relationship is postulated, where the slope increases with increasing concentration.

Droplet Resistance (R_DROPLET) vs. Wetted Area

- DI Water
- 0.1M NaCl
- 0.6M NaCl

$y = 82.948x^{-0.507}$
$R^2 = 0.944$

$y = 4.1445x^{-0.441}$
$R^2 = 0.9863$

$y = 4.1357x^{-0.427}$
$R^2 = 0.98$

Resistance, kilo-Ω

Droplet Contact Area, mm^2
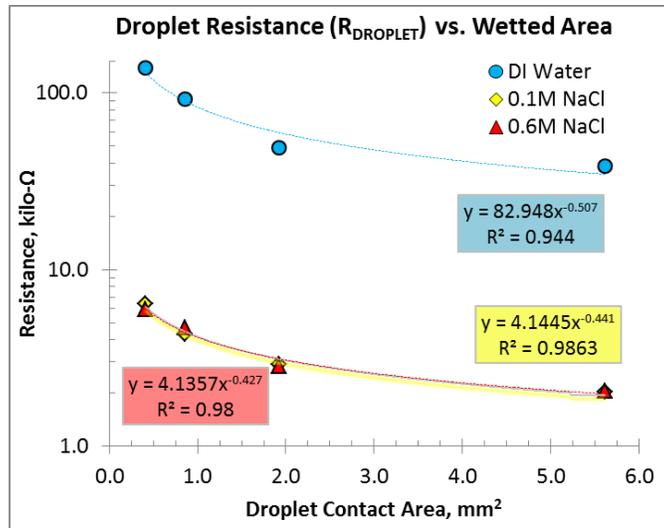
Figure 15: Droplet Resistance ($R_{DROPLET}$) vs. volume; negative logarithmic trend with increasing volume is postulated; overall resistance values decreasing as concentration increases.

Deliquescence of Dry Salt Particles in an Increasing %RH Atmosphere

The sensor was tested under changing humidity conditions, with dried salt deposits present. Salt particles, created by air-drying a 1.0µL droplet of 1.0 M NaCl, are shown in Figure 16. Visual estimation and comparison of the large salt particles to the dimensions of the sensor components showed that the particles deposited in this method were greater than about 50 µm in diameter (or greater than 50 µm in the longest dimension for irregularly-shaped particles); dimensions varied widely above that estimation. In the deliquescence experiment, the %RH in the chamber was rapidly changed by adding approx. 150 mL DI water to the control solution (10 mL). This resulted in an increase in humidity from about 33%RH (the equilibrium for air above saturated $MgCl_2$) to about 85%RH. Figure 17 shows digital camera images taken at various %RH points during the humidity increase. The deliquescence shown between 60%RH and 74.5%RH corresponds to the marked decrease in overall Z_{MOD} and the transition from capacitive (phase closer to -90°) to resistive (phase closer to 0°) behavior shown in Figure 18.
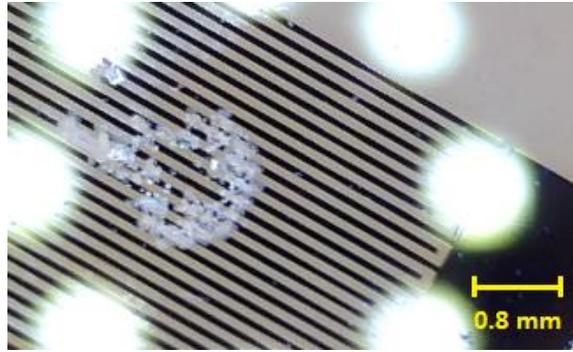
Figure 16: Approximate size of the dried salt deposit used in deliquescence test.
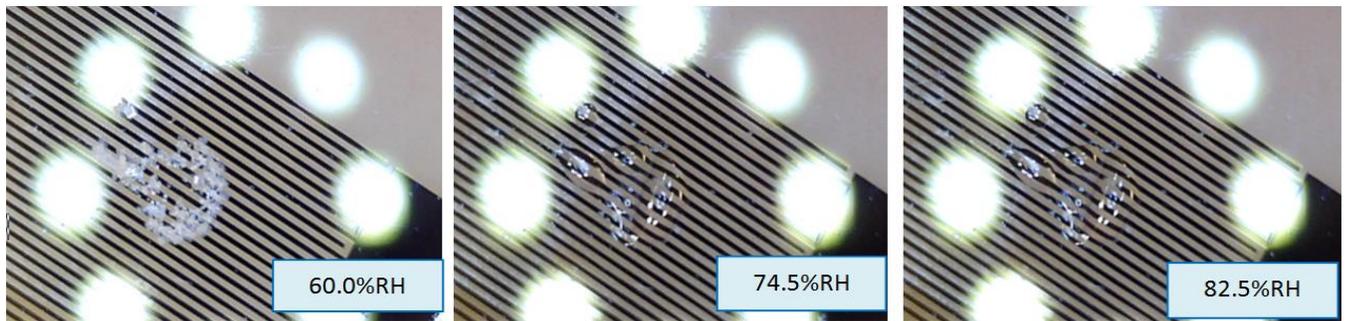
Figure 17: Digital camera images showing deliquescence of NaCl crystals as %RH increases.
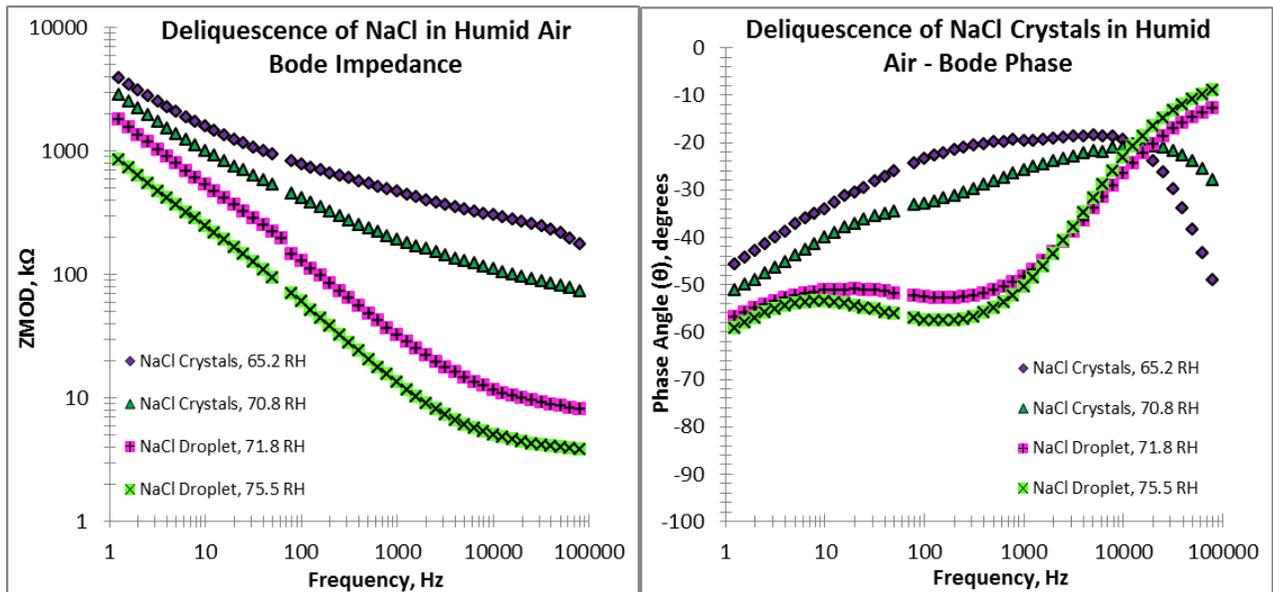
Figure 18: Bode impedance (left) & phase (right) during deliquescence.

As before, EIS-fitting, (Fig. 7(B)) was used to identify changes in the sensor's equivalent circuit parameters. The results of fitting analysis were most significant for $R_{DROPLET}$ and $C_{DROPLET}$, as summarized in Figure 19. As humidity increases to about 75%RH, the salt crystals (previously non-conductive) become wetted, and the capacitance increases, while the resistance decreases. As shown in Figures 18 & 19, deliquescence was observed in the range of 71-75%RH.
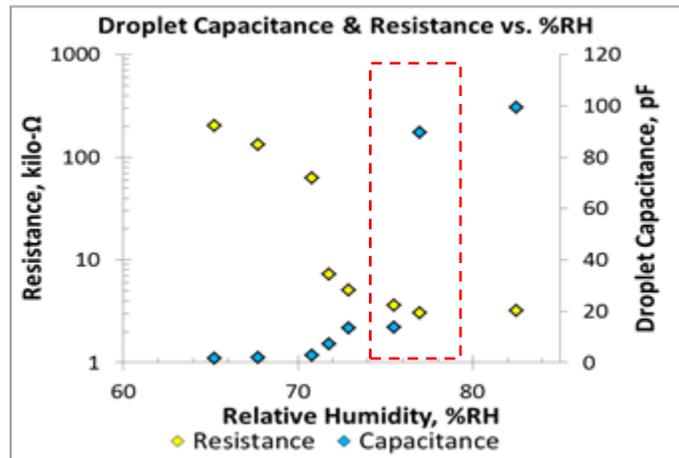
Figure 19: Changes in $C_{DROPLET}$ and $R_{DROPLET}$ in the range of 71-75%RH.

Discussion/Analysis

Preliminary testing under controlled laboratory condition demonstrates the sensitivity and accuracy of the IDT sensor for improved TOW measurement. *Sensitive* means that the sensor responds to changes in volume, concentration, etc. of the droplet. *Accurate* indicates that the sensor very reliably detects wetness events, including differentiation between a dry salt and hydrated salt on the surface. Examples of sensor inaccuracy would include (1) true wetting events not recorded by the sensor, and (2) the indication of wetting by the sensor when no true event occurs. Many current sensors measure galvanic current, resistance, or electrical impedance

between interwoven electrodes to determine whether or not a material is "wet," [5,7]. Wetness is evaluated by comparing the output to a threshold value.

Trends proposed in Figures 13 through 15 suggest linear relationships between droplet contact area and both $C_{DROPLET}$ and Q_{dl}, and a logarithmic relationship between $R_{DROPLET}$ and contact area. These trends are not proven through robust experimentation in this work. They are only presented because plots of these circuit parameters suggest such trends. Based on the proposed equivalent circuit model discussed previously, the data points observed (on both impedance vs. frequency and phase delay vs. frequency) agree with the theoretical equivalent circuit proposed in this work and based in other literature. The agreement between the predicted impedance (from equivalent circuit fitting) and measured data points breaks down only slightly and the highest and lowest decade of frequencies in the spectrum examined, for saltwater electrolytes.

As shown in Figures 18 & 19, deliquescence was observed in the range of 71-75%RH. The room temperature deliquescence RH is traditional reported as exactly 75.3%RH[4] or approximated as 75%RH[12,13,14] at room temperature. Discrepancy between observed and literature deliquescence RH may be due to fast rate of RH increase in the test, or distance between the TOW sensor & RH meter in the chamber. Deliquescence of salt crystals on a surface can also have the effect of lowering the local RH near the surface[3]. Below the deliquescence point, there is no volume or concentration change; only dry salt crystals are present on the surface. Above this point, concentration will decrease as the volume increases with increasing RH. Changes in behavior above the deliquescence %RH have not been evaluated.

Proposal of Alternative Equivalent Circuit Model

As discussed previously, the phase delay in the circuit of the wetted sensor is not fully realized using only the Q_{DL} effective capacitance; addition of $C_{DROPLET}$ incorporates effects of bulk solution, as in Lvovich & Smiechowski [15]. The phase delay from $C_{DROPLET}$ may be related to water polarity alignment [16]. Thus, a new equivalent circuit is proposed, incorporating $R_{DROPLET}$ & $C_{DROPLET}$, in parallel, between a pair of equivalent metal-electrolyte interface circuits, each with Q_{DL} and R_P (polarization resistance, previously omitted), Figure 20.
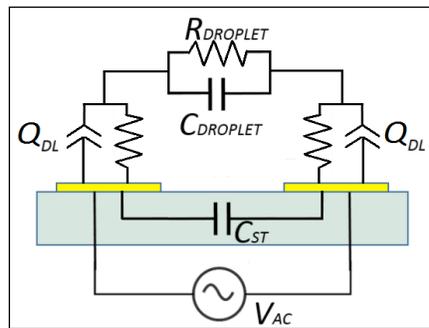
Figure 20. Proposed equivalent circuit, to be used in further examinations.

Design of an IDT sensor array

The current phase of this work includes the development of a 1X5 linear sensor array. This design will serve as a proof of concept of the multiplexed array sensor, in 1-dimension. The design uses a single AC voltage perturbation from the potentiostat, exciting a conductor common to all 5 IDT sensors in the linear array. The response will be selected form one of the five IDTs by the use of a time-multiplexer, such that information from only one array is interrogated at a time. A sketch is presented in Figure 21. Experimentation with the 1X5 linear array will guide the further development of a 5X5 matrix array sensor. While the linear array requires only one multiplexer and a single layer of photolithgraphically deposited metal on the substrate, the matrix

array is more complex. A possible schematic of the 5X5 array is shown in <u>Figure 22</u>, although multiple options are being explored to obtain the best design while maintaining efficient signal processing. Both a linear or matrix array sensor could determine the area fraction, electrolyte concentration, and duration of wetness across a surface, providing more information than a single-IDT sensor, in the case of non-uniform wetting phenomena.
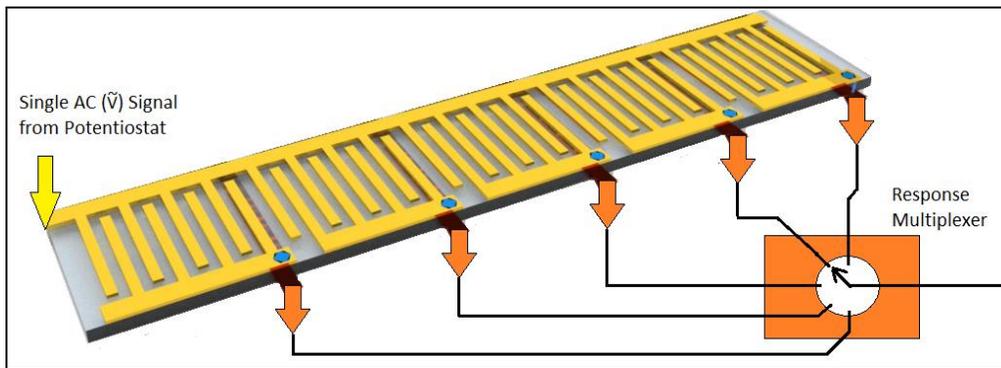
<u>Figure 21</u>: Design schematic of Linear 1X5 array under development.
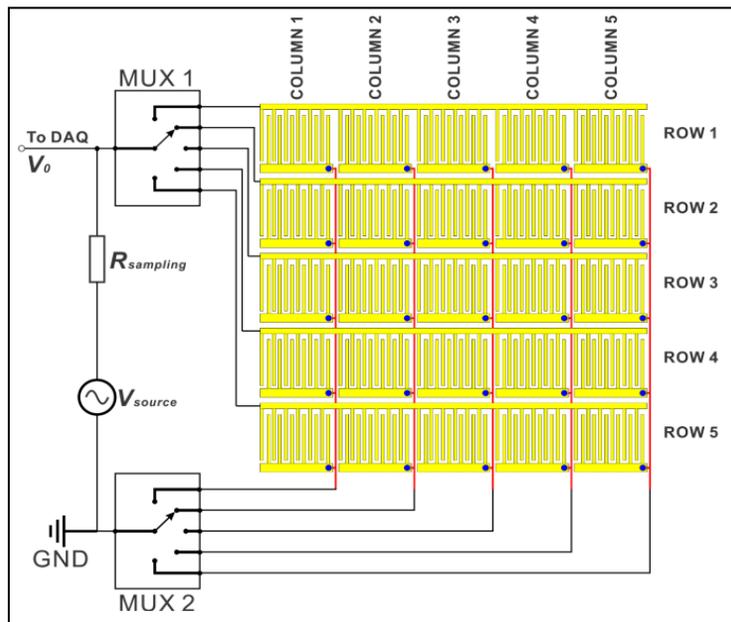
<u>Figure 22</u>: Design schematic of Matrix 5X5 array, long-term project goal.

Our goal of a multiplexed IDT-sensor array is a proposed improvement over current sensors. The use of impedance spectra to characterize droplet size and concentration provides more information than current technology options, which output a binary result: *wet* or *dry*. Data analysis methods suggest that equivalent circuit parameters may exist (i.e. $C_{DROPLET}$) which could allow the salinity & size of an electrolyte droplet to be measured separately from the electrodes' double layer capacitance (Q_{DL}). However, additional investigation is required for both more concentrated and more dilute concentrations of salt water, as well as additional droplet sizes. A variety of electrolyte species (i.e. salt solutions other than NaCl) should also be examined to test the relationships proposed.

Conclusions

TOW, %RH, and other variables affect atmospheric corrosion reactions greatly. Current TOW sensors and associated data analysis methods are limited in accuracy and sensitivity. A new IDT-based sensor array is proposed in this work. Characterization tests for a variety of droplet sizes and electrolyte concentrations were conducted with a single-IDT sensor, fabricated photolithographically from chromium. Analysis of the impedance spectra, using equivalent circuits proposed previously in this work allows the determination of circuit parameters that may be functions of droplet size and electrolyte concentration. The interrogation of the sensor at many frequencies could afford for the simultaneous determination of wetted area and conductivity of electrolyte. However, experimentation with alternative electrolyte species, broader concentration ranges, and various droplet volumes are necessary to corroborate these initial conclusions. An alternative equivalent circuit, accounting for the effects of metal-solution interface (Q_{DL} & R_P) in series with the bulk effects ($C_{DROPLET}$ & $R_{DROPLET}$), is also suggested, and will be the subject of ongoing investigation.

Observation of these trends suggests that it is possible to differentiate between different sizes of droplets and concentrations of electrolytes on the single-IDT sensor. Two designs for a novel sensor array are proposed, with multiple IDT sensors arranged in both 1-D (1X5) and 2-D (5X5). These array designs seek to successfully characterize non-uniform wetting conditions across a surface.

Appendix A – Evaluation of Wetted Area Effect

The following section was appended to this Honors Project report at the recommendation of a reader/reviewer, to examine whether fitted model results match expected behavior.

To test the validity of the model, normalization was performed with respect to the approximated wetted metal area, A_{WM}, for each of the different sized droplets; A_{WM} is expressly different from the droplet contact area, A_C, discussed previously, since A_C was only concerned with estimating the surface area under the droplet (including wetted area of the polyimide sensor substrate, A_{WS}). Normalization of fitted equivalent circuit parameters is simplest for Q_{DL}, since this parameter is directly related to A_{WM}; it is expected that, for the same electrolyte concentration, the normalized Q_{DL} (i.e. $\hat{Q}_{DL}$) values will be approximately equal between the different droplet sizes. To some extent, $R_{DROPLET}$ is closely related to A_{WM}, since $R_{DROPLET}$ includes both R_P (polarization resistance) and R_S (solution resistance), both of which in included in the traditional Randle's circuit. $C_{DROPLET}$ is much more complex than $R_{DROPLET}$, since the electric field carried in the solution is geometrically complex. Despite difficulties and possible incongruences with the equivalent circuit, normalization is nonetheless performed for all circuit parameters: Q_{DL}, $C_{DROPLET}$, and $R_{DROPLET}$.

The easiest method to approximate the exposed metal area, A_{WM}, is a graphical method that simply uses the scale bar from digital camera images taken during representative droplet tests. Once the total length of the wetted sensor elements is measured (in μm), A_{WM} is found by multiplying this length by 71 μm (since each unit length of sensor linear element is 70 μm across

the top and has an approximate height off the substrate of 0.5 µm on each edge). Figure A1 shows this method. Unfortunately, the pictures taken with the digital camera for droplets of 0.3, 1.0, and 5.0 µL did not include the entire droplet within the bounds of the image (see Figure 8 in report). Thus, it is not possible to measure the length of the electrodes under the droplet but not contained within the image. An example calculation is shown in Table A1, for the 0.1 µL case.
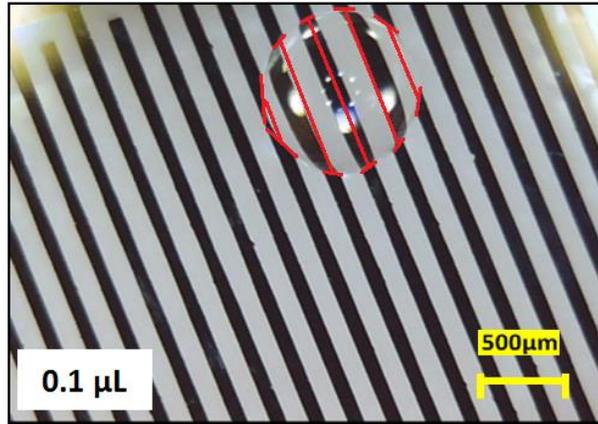
Figure A1. 0.1 µL droplet, showing method for measuring A_{WM} graphically.

Table A1. Example Calculation of AWM for the 0.1 µL droplet (only volume possible)

ΔX	ΔY	Pixels	Length, µm
13	22	25.6	170
44	109	117.5	784
50	122	131.8	879
45	111	119.8	798
27	63	68.5	457
	Legend:	75	500
	Total Meas. Length	**Total Wetted Metal Area**	**Units**
	3088	2.193E+05	µm^2
		0.2193	mm^2

Due to the limitations of the graphical method, an alternative method for estimating the wetted metal area is proposed, as follows. Recall that the contact areas of tested volumes were approximated assuming hemispherical droplets. The radius of the wetted area beneath each

droplet can be found, $R = \sqrt{A/\pi}$. Considering the linear elements of the sensor, the lengths of each element contained within this are can be approximated as a chord. The length of the chord, a, is given by $a = 2R \sin\left(\frac{\theta}{2}\right)$, where θ is the angle from the center of the circle to the two ends of the chord, given by $\theta = 2\cos^{-1}\left(\frac{r}{R}\right)$, where r is the perpendicular distance from the circle center to the chord. Therefore, the length of any given chord, a_i, is given by the equation $a_i = 2R\left(\sin\left(\cos^{-1}\left(\frac{r}{R}\right)\right)\right)$. Notably, r need not be measured graphically. Since the radius of the wetted circle under the droplet (R) is known, and the electrodes, including the gaps between elements, are 150μm apart on center, the approximate number of elements, n, under the droplet is given by $n = \frac{2R}{150}$ where R has units of microns. The chord at $i = 1$ (i.e. $\frac{i}{n}R = r$) will correspond to the full diameter, or longest wetted portion of any element under the droplet. The chord at $i = n$ (i.e. $\frac{n}{n}R = r$) will correspond to the shortest. The indexing ($i's$) of the chords is not ordered from one end of the wetted circular area to the other, but rather is automatically in order of increasing length. The total length of wetted sensor elements is thus given by $L = \sum_{i=1}^{n} 2R\left(\sin\left(\cos^{-1}\left(\frac{i}{n}\right)\right)\right)$, and the area of wetted metal is $A_{WM} = 71 \cdot L$. This approximation requires that the droplets used in the experiments straddle only the interlocking linear 'finger' regions of the sensor; it would not be a valid approximation if a large portion of the wetted area were on one of the sensor's 'headers' from which the linear elements extend. The summations for wetted length are easily computed using a TI-89 calculator. The results of the A_{WM} calculated in this manner (a.k.a. "Method 1") are presented in Table A2.

Table A2. Calculated (Method 1) results for wetted metal area (A_{MW}) under the droplets.

Droplet Size	Contact Area	Radius, R	Elements, n	Wetted length	A_{WM}
μL	mm^2	μm	-	μm	mm^2
0.1	0.4135	362.8	5	2392	0.1698
0.3	0.8601	523.2	7	5114	0.3631
1	1.919	781.6	11	12585	0.8936
5	5.612	1337	18	36267	2.575

Another defensible approximation of wetted area stems – and simpler – is to assume that every 70-µm wide sensor element is matched in length by an adjacent 80-µm sensor gap. Then, for a large enough droplet, the fraction of wetted metal within the droplet will equal $\frac{70}{150} A_c$, where A_c is the contact area presented in Table 1 of the report. This method is dubbed "Method 2" It would even more correct to add in the edges of the elements, although this changes the calculated wetted metal area, A_{WM}, very little. Since this approximation method is pursued primarily for its simplicity, this correction is not performed. Table A3 compares the different methods discussed above for area calculation. Inspection of the table demonstrates that the methods are in good agreement, for the purposes of the normalization to be performed. Due to its elegance, the summation method is elected for continued analysis. Due to the assumptions made in all three area-approximation methods, the relative error in estimated A_{WM} always decreases with increasing droplet size.

Table A3. Comparison of calculated A_{WM} results by different methods

Method -->	1	2	Graphical
Droplet Size, µm	mm^2	mm^2	mm^2
0.1	0.1698	0.1930	0.2193
0.3	0.3631	0.4014	N/A
1	0.8936	0.8956	N/A
5	2.575	2.619	N/A

Table A4 presents normalized values for applicable circuit parameters. Normalized values for double layer effective capacitance, $\hat{Q}_{DL}$, should be the same within a given electrolyte. Clearly, observation of the table values demonstrates that for DI water and $0.1M$ NaCl electrolytes, this expectation is met. However, for $0.6M$ NaCl electrolyte, the expectation is not observed. This is an indication that the model employed in the equivalent circuit analysis has room for improvement, particularly with concern to more concentrated electrolytes. The shortcomings of the present model may be associated with the omission of polarization resistance, R_P, or with the series/parallel order of circuit elements. Next consider $R_{DROPLET}$, based on the equivalent circuit used in the fitting (Figure 7 in report), this resistor is in series with the two Q_{DL} constant phase elements. Due to this construction, it is not purely correct to separate the impedances of the $R_{DROPLET}$ components – R_P & R_S - linearly, since they are not simply in series with one another. However, as an academic exercise, not only is this simple normalization performed anyway, for each of the electrolyte concentrations, a fraction, f, is solved to minimize the standard deviation in the normalized $R_{DROPLET}$ values, and approximate a contribution to $R_{DROPLET}$ coming from both R_P & R_S. The f values used for this test are shown in Table A5. In the case of $C_{DROPLET}$, since we are not dealing with a perfect parallel plate capacitor, normalization has relatively little meaning in comparing the results within a given electrolyte concentration. $C_{DROPLET}$, related to the electric field carried by the electrolyte, is a much more complex function of A_{WM}, droplet height, and other variables, than is Q_{DL}.

Table A4. Normalized Values for All Fitted Equivalent Circuit Parameters.

	Droplet Size	Contact Area	Q_{DL}	Normalized Q_{DL}	n	$R_{DROPLET}$	Normalized $R_{DROPLET}$	$R_{DROPLET}$ Optimized	$C_{DROPLET}$	Normalized $C_{DROPLET}$
	μL	mm^2	$nF\cdot s^{(n-1)}$	$nF\cdot s^{(n-1)}\cdot mm^{-2}$	No units	$K\Omega$	$K\Omega\cdot mm^2$	$K\Omega\cdot mm^2$	pF	$pF\cdot mm^{-2}$
DI Water	0.1	0.4135	19.26	113.4	0.55639	138.01	23.44	71.37	2.807	16.53
DI Water	0.3	0.8601	52.25	143.9	0.54721	92.3	33.51	58.11	3.775	10.40
DI Water	1	1.9192	90.33	101.1	0.56937	48.72	43.53	45.70	5.419	6.065
DI Water	5	5.6117	230.49	89.51	0.53046	38.596	99.38	73.95	11.739	4.559
0.1 M NaCl	0.1	0.4135	19.6	115.4	0.67345	6.422	1.091	3.709	0.823	4.846
0.1 M NaCl	0.3	0.8601	47.33	130.4	0.64554	4.305	1.563	2.910	3.606	9.932
0.1 M NaCl	1	1.9192	106.61	119.3	0.62365	2.904	2.595	2.747	6.827	7.640
0.1 M NaCl	5	5.6117	352.07	136.7	0.60856	2.033	5.235	3.663	25.46	9.887
0.6 M NaCl	0.1	0.4135	84.34	496.6	0.59261	5.982	1.016	3.566	3.378	19.89
0.6 M NaCl	0.3	0.8601	131.62	362.5	0.58844	4.703	1.708	3.246	7.277	20.04
0.6 M NaCl	1	1.9192	179.6	201.0	0.59458	2.855	2.551	2.707	9.402	10.52
0.6 M NaCl	5	5.6117	511.8	198.8	0.60141	2.052	5.284	3.624	33.93	13.18

Table A5. Fraction of $R_{DROPLET}$ contributed by solution resistance, R_S

	DI Water	**0.1 M NaCl**	**0.6 M NaCl**
$\sigma(R_{DROPLET})$	13.05	0.4999	0.4201
R_S **fraction,** f	0.4183	0.4911	0.5135

Literature Cited

[1] S. W. Dean, D. B. Reiser, "Time of Wetness and Dew Formation: A Model of Atmospheric heat Transfer." *Atmospheric Corrosion, ASTM STP 1239*. W. W. Kirk & H. H. Lawson, Eds. (Philadelphia PA: ASTM International, 1995), 3-10.

[2] E. Schindelholz, R.G. Kelly, I.S. Cole, W.D. Ganther, T.H. Muster, "Comparability and accuracy of time of wetness sensing methods relevant for atmospheric corrosion," *Corrosion Science*, 67, (2013): 233-241

[3] P. Norberg, "Surface Moisture and Time of Wetness Measurements." In *Service Life Prediction Methodology and Metrologies, ACS Symposium Series 805*. J. W. Martin & D. R. Bauer, Eds. (Washington, D.C.: American Chemical Society, 2002), 23-36.

[4] I. S. Cole, W. D. Ganther, J. D. Sinclair, D. Lau, D. A. Paterson, "A Study of the Wetting of Metal Surfaces in Order to Understand the Processes Controlling Atmospheric Corrosion," *J. Electrochemical Soc.,* 151, 12, (2004): B627-635.

[5] D. Mizuno, S. Suzuki, S. Fujita, N. Hara, "Corrosion monitoring and materials selection for automotive environments by using Atmospheric Corrosion Monitor (ACM) sensor," *Corrosion Science*, 83, (2014): 217-225.

[6] ASTM[1] G 92-86 (2015), "Standard Practice for Characterization of Atmospheric Test Sites" (West Conshohocken, PA: ASTM).

[7] ASTM[1] G 84-89 (2012), "Standard Practice for Measurement of Time-of-wetness on Surfaces Exposed to Wetting Conditions in Atmospheric Corrosion Testing" (West Conshohocken, PA: ASTM).

[8] D. A. Jones, "Atmospheric Corrosion and Elevated Temperature Oxidation." In *Principles and Prevention of Corrosion, 2nd Ed.* Prentice-Hall: (Upper Saddle River, NJ: Prentice Hall, 1996): 399-408

[9] Z. Y. Chen, F. Cui, R. G. Kelly, "Calculations of the Cathodic Current Delivery Capacity and Stability of Crevice Corrosion under Atmospheric Environments." *J. Electrochemical Soc.,* 155 (7), (2008):C360-368

[10] E. Schindelholz, L. Tsui, R. G. Kelly, "Hygroscopic Particle behavior Studied by Interdigiated Array Microelectrode Impedance Sensors," *J. Physical Chemistry A*, 188, (2014): 167-177.

---

[1] ASTM International, 100 Barr Harbor Dr., West Conshohocken, PA 19428-2959.

[11] A. R. Barron, "5.6 – Optical Issues in Photolithography," In *Chemistry of Electronic Materials* A. Barron (Rice University Openstax, 2009), 9 Sept 2012, http://cnx.org/contents/EJYWe4UY@9.3:_WZH864Z@1/Photolithography (11 Sept 2016).

[12] J. C. W. Frazer, R. K. Taylor, A. Grollman, "Two-phase liquid-vapor isothermal systems, vapor pressure lowering." In *Core Historical Literature of Agriculture: International Critical Tables, Vol III* (1928): 292-309.

[13] S. Li, L. H. Hihara, "Aerosol Salt Particle Deposition on Metals Exposed to Marine Environments: A Study Related to Marine Atmospheric Corrosion," *Journal of The Electrochemical Society*, 161, 5 (2014): C268-C275

[14] I. S. Cole, W. D. Ganther, "Experimental determination of duration of wetness on metal surfaces," *Corrosion Engineering, Science and Technology*, 43, 2 (2008): 156-162

[15] V. F. Lvovich, M. F. Smiechowski, "AC Impedance Characterization of Highly Resistive Media Using Four-Electrode Electrochemical Cells" *ECS Transactions,* 25, 32 (2010): 1-25

[16] G. L. Johnson, "Chapter 3 – Lossy Capacitors" In *Soild State Tesla Coil* (2001): 3.1-3.24

[17] NACE International, "International Measures of Prevention, Application, and Economics of Corrosion Technologies Study" Report No. OAPUS310GKOCH; 2016.